Evaluation of Warm-Rain Microphysical Parameterizations in Mesoscale Simulations of the Cloudy Marine Boundary Layer

KEVIN J. NELSON AND DAVID B. MECHEM

Department of Geography and Atmospheric Science, University of Kansas, Lawrence, Kansas

YEFIM L. KOGAN

Cooperative Institute for Mesoscale Meteorological Studies, University of Oklahoma, Norman, Oklahoma

(Manuscript received 30 July 2015, in final form 2 January 2016)

ABSTRACT

Several warm-rain microphysical parameterizations are evaluated in a regional forecast model setting (using the Naval Research Laboratory's Coupled Ocean–Atmosphere Mesoscale Prediction System) by evaluating how accurately the model is able to represent the marine boundary layer (MBL). Cloud properties from a large suite of simulations using different parameterizations and concentrations of cloud condensation nuclei (CCN) are compared to ship-based observations from the Variability of the American Monsoon Systems (VAMOS) Ocean–Cloud–Atmosphere–Land Study—Regional Experiment (VOCALS-REx) field campaign conducted over the southeastern Pacific (SEP). As in previous studies, the simulations systematically underestimate liquid water path and MBL cloud depth. On the other hand, the simulations overestimate precipitation rates relative to those derived from the scanning C-band radar on board the ship. Most of the simulations exhibit a diurnal cycle, although details differ somewhat from a recent observational study. In addition to direct comparisons with the observations, the internal microphysical consistency of simulated MBL cloud properties is assessed by comparing simulation output to a number of observationally and theoretically derived scalings for precipitation and coalescence scavenging. Simulation results are broadly consistent with these scalings, suggesting COAMPS is behaving in a microphysically consistent fashion. However, microphysical consistency as defined in the analysis is highly dependent upon the horizontal resolution of the model. Excessive depletion of CCN from large coalescence processing rates suggests the importance of parameterizing a source term for CCN or imposing some form of fixed, climatological background CCN concentration.

1. Introduction

Marine boundary layer (MBL) clouds substantially affect the moisture and energy budgets of the Earth's atmosphere (Krueger et al. 1995; Leach and Raman 1995). On average, stratocumulus clouds off the western continental coasts cover approximately 34% of the world's oceans (Klein and Hartmann 1993). These persistent low clouds remain a source of substantial uncertainty in climate models (Bony and Dufresne 2005; Medeiros et al. 2008; IPCC 2013), and on shorter time scales produce drizzle and fog, which can affect maritime and aviation operations (Mechem and Kogan 2003).

MBL cloudiness is not characterized by a single cloud type but rather by a continuum of cloud regimes and transitions. Oceanic cloud regimes transition from unbroken stratocumulus near the coast, to open-cell shallow (trade) cumulus farther west, followed by cumulus congestus and deep convection in the western tropical oceans (Albrecht et al. 1995; Stevens 2005). Because many of the processes that occur in clouds (lateral and cloud-top entrainment, microphysical processes) are smaller than a mesoscale model grid volume, they must be parameterized (McCaa and Bretherton 2004; Wang et al. 2011). Regional forecast (mesoscale) models have consistently struggled with accurately representing MBL cloud processes.

Rahn and Garreaud (2010a,b) compared output from the Weather Research and Forecasting (WRF) Model with observations from the Variability of the American Monsoon Systems (VAMOS) Ocean–Cloud–Atmosphere–Land Study—Regional Experiment (VOCALS-REx;

Corresponding author address: D. B. Mechem, Dept. of Geography and Atmospheric Science, University of Kansas, 1475 Jayhawk Blvd., Room 213, Lawrence, KS 66045.
E-mail: dmechem@ku.edu

DOI: 10.1175/MWR-D-15-0266.1

Wood et al. 2011; Mechoso et al. 2014), and found that MBL depth varied little along the coast. An east–west gradient in sea surface temperature (SST) leads to a corresponding east–west gradient of MBL depth, with the deeper MBL farther west (Rahn and Garreaud 2010b). Zonal flow in the southeast Pacific (SEP) is minimal, and the lower-tropospheric meridional flow is predominantly southerly, which contributes to the northward movement of continental aerosols. Toniazzo et al. (2011) corroborate the findings of Rahn and Garreaud (2010a,b) and also demonstrate that a midlatitude cyclone caused the advection of high aerosol concentration early in November 2008.

Wang et al. (2011) conducted real-time forecast simulations during VOCALS using the Naval Research Laboratory's (NRL) Coupled Ocean–Atmosphere Mesoscale Prediction System (COAMPS; Hodur 1997). Wang et al. found that COAMPS consistently underestimated liquid water path (LWP) of nearshore clouds and MBL depth. Because synoptic forcing during the VOCALS field campaign was weak, the negative biases in LWP and MBL depth likely arise from errors in how the MBL subgrid-scale (SGS) dynamics and microphysics are represented in the model. Wang et al. also show significant improvements to the model output when simulations are run with grid spacings less than or equal to 5 km in the horizontal. Increasing horizontal resolution in their simulations ($\leq$5 km) reduced relative error by 25%–50% for MBL depth and cloud water mixing ratio q_c.

Even in high-resolution simulations, however, poor treatment of microphysical processes can lead to overproduction of precipitation, corrupting the diurnal cycle of cloud properties (Boutle and Abel 2012). Running the Met Office Unified Model (MetUM) for a 2-day period during the VOCALS field campaign, Boutle and Abel found that cost-effective improvements to the microphysical parameterization, such as replacing the autoconversion formulation or modifying the raindrop size distribution, can result in substantial improvements to cloud-system behavior.

While the ability of numerical weather prediction (NWP) models to represent MBL cloud systems has improved since their inception, the drawbacks of using single-moment microphysics parameterizations such as Kessler (1969) or Manton and Cotton (1977) for boundary layer clouds are well known (Baker 1993; Chen and Cotton 1987). Single-moment parameterizations only account for mixing ratios of the different states of water. For example, the Kessler (1969) parameterization employs an artificial Heaviside threshold function for autoconversion and fall speed relations tuned for convective environments (Kessler 1995; Khairoutdinov and Kogan 2000; Liu et al. 2005). These drawbacks prompted the development of double-moment parameterizations such as those from Khairoutdinov and Kogan (2000), Liu and Daum (2004), Morrison et al. (2005a,b), and Seifert and Beheng (2006), which sought to alleviate some of the deficiencies of single-moment parameterizations. Double-moment parameterizations account for water mixing ratios like single-moment parameterizations but also include droplet concentrations. Hybrid schemes are also possible, in the form of single-moment parameterizations that borrow components (such as the autoconversion formulations) from double-moment schemes (Boutle and Abel 2012; Hill et al. 2015).

Using droplet spectra from aircraft observations, Wood (2005) evaluated microphysical process rates from six different parameterizations by comparing autoconversion and accretion rates calculated from the parameterizations with those calculated directly from the observations using the stochastic collection equation (SCE). They found that the different formulations for autoconversion exhibited the greatest discrepancies between parameterization and SCE calculations, with several of the double-moment parameterizations outperforming single-moment parameterizations. Mechem and Kogan (2003) compared the performance of the Khairoutdinov and Kogan (2000) double-moment parameterization to the operational single-moment parameterization in the operational version of COAMPS. They found that the double-moment parameterizations promote the emergence of mesoscale variability characteristic of a drizzle-induced cloud-regime transition from well-mixed stratocumulus to a more decoupled, broken cloud system. Thus, the double-moment parameterizations lead to more physically realistic cloud-system behavior relative to the simpler, single-moment microphysical treatments. A comprehensive examination of a number of single and double microphysical parameterizations (including those we evaluate in our study), forced by common dynamics, confirms the utility of the double-moment parameterizations, and that advantages of tuning singe-moment parameterizations (e.g., adjusting details of rain production) are limited (Hill et al. 2015).

Observations collected during the VOCALS-REx field campaign give us a prime opportunity to evaluate the performance of warm-rain microphysical parameterizations in a mesoscale model setting. We conduct multiday COAMPS simulations for a period during the VOCALS field campaign and perform an extensive comparison of the simulation results to VOCALS observations for a number of warm-rain microphysical parameterizations. In addition to a direct comparison with the VOCALS observations, we evaluate the internal microphysical consistency of the simulations by assessing how the results adhere to observationally derived scalings for precipitation rate and coalescence scavenging (the reduction of cloud-droplet

concentration accompanying the collision–coalescence process). We demonstrate that the double-moment parameterizations tested here generally behave similarly for this particular case and that model behavior for most of these parameterizations is microphysically consistent. The evaluation of microphysical consistency through the precipitation and coalescence-scavenging scalings gives valuable insight into the resolution dependence of simulation results beyond the basic comparison between model and observations.

2. Methodology

a. Model and domain configuration

All simulations employ NRL COAMPS (Hodur 1997), which is based on nonhydrostatic, compressible dynamics. COAMPS integrates acoustically active terms using a mode-splitting technique and uses a 1.5-order "level 2.5" turbulence closure (Mellor and Yamada 1982) for boundary layer and subgrid-scale dynamics, with modifications suggested by Burk and Thompson (1989). COAMPS uses the Louis et al. (1982) parameterization to calculate surface fluxes. Deep convective processes are parameterized using Kain and Fritsch (1990), although in marine stratocumulus regions, instability is never sufficient to trigger the parameterization. Shortwave and longwave radiative transfer are performed using the parameterization of Fu and Liou (1992), as implemented by Liu et al. (2009). Details about the microphysical parameterizations in COAMPS are given below in section 2c. COAMPS is not equipped with a subgrid-scale cloudiness parameterization, so grid volumes are assumed to be either completely clear or completely saturated, an assumption well understood to lead to biases in nonlinear microphysical process rates like autoconversion (Pincus and Klein 2000; Larson et al. 2001; Wood et al. 2002; Kogan and Mechem 2014; Boutle et al. 2014a). All parameterizations are active across all the grids, except for the deep convective parameterization, which is switched off for horizontal grid spacings smaller than 10 km.

COAMPS simulations were conducted for a specific period during VOCALS to promote comparisons with observations. We chose the period from 12 to 16 November 2008 when the NOAA R/V *Ronald H. Brown* (hereafter *RHB*) was on station (20°S, 75°W) collecting observations. COAMPS was configured so that the nested model domains were centered on the location of the *RHB* during this time. We chose to use three nested domains with horizontal grid spacings of 27, 9, and 3 km, and grid sizes of 127 × 127, 91 × 91, and 91 × 91, respectively. The time steps for the three grids are 60, 20, and 6.67 s, respectively. Figure 1 shows the bounds of each nest, and the purple star at the center represents the location of the *RHB* during the simulation period. We follow Wang et al. (2011) and use the same 45-level vertical grid spacing, which is a trade-off between high resolution and operational computational feasibility. The vertical grid spacing ranges from 20 to 60 m throughout much of the boundary layer and then increases to 150 m for a depth of several hundred meters (Fig. 1). We test the dependence of MBL cloud properties on the vertical grid by increasing the number of grid points in the MBL by 10 (from 45 to 55 points in total), an increase that makes little difference in simulation results. Vertical resolution is important, of course, and large increases in the number of vertical grid points would undoubtedly improve aspects of the simulations. However, because COAMPS is an operational model, our grid configuration choices do not stray too far from operational feasibility.

The NRL's operational global model Navy Operational Global Atmospheric Prediction System (NOGAPS) provides initial and boundary conditions for COAMPS at 6-h intervals. The COAMPS initial conditions and update cycles also incorporate additional observations through data assimilation. Only basic thermodynamic fields (geopotential height, potential temperature, and mixing ratio) and horizontal momentum are assimilated; hydrometeor fields are not included. Lateral boundary conditions are imposed over an outer seven-point border of each grid using the method of Davies (1983). A 24-h spinup period, consisting of two model update cycles, was run to develop boundary layer thermodynamic and cloud structure.

b. Observations during VOCALS-REx

The VOCALS field campaign was a multiplatform airborne, ship-, and land-based observational campaign intended to sample the southeast Pacific stratocumulus-topped boundary layer and lower free troposphere from 16 October to 15 November 2008 (Bretherton et al. 2010; de Szoeke et al. 2010). Our research uses a subset of data from the second cruise (12–16 November 2008), as described in de Szoeke et al. (2010) and de Szoeke et al. (2012). LWP was retrieved from microwave brightness temperatures observed by vertically pointing microwave radiometers as described in Zuidema et al. (2005). Laser ceilometers measured the cloud-base height, and surface quantities (i.e., temperature, humidity, heat, and moisture fluxes) were obtained from instruments mounted on a mast at the front of the ship (de Szoeke et al. 2010). A CCN counter supplied estimates of CCN concentration at 0.6% supersaturation (Wood et al. 2011; D. Covert 2009, unpublished data). Rain rates over the subcloud layer were calculated from radar reflectivity factor sampled from a scanning C-band radar on board the *RHB* (Comstock et al. 2004; Burleyson et al. 2013). Rain-rate retrievals include uncertainty estimates corresponding

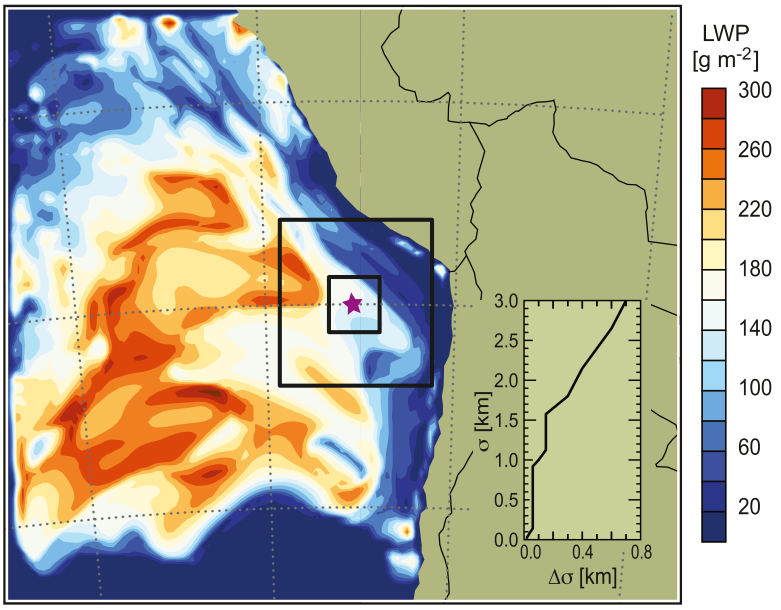

FIG. 1. Filled contour plot of LWP for the K2013 parameterization at a simulation time of $t = 72$ h. Inner bold lines show the second and third nests, respectively. The purple star indicates the location of the *RHB* throughout the simulation period. The vertical grid configuration is inset on the LWP plot.

to a ±2-dBZ uncertainty in radar calibration. We chose to use the C-band radar instead of the W-band cloud radar in order to be able to quantify the spatial variability of precipitation within the VOCALS domain.

Remote sensing observations from the Moderate Resolution Imaging Spectroradiometer (MODIS; Justice et al. 1998) products were employed to assess the degree of horizontal variability of MBL aerosol over the SEP. Unfortunately, MODIS aerosol products (Remer et al. 2005) are column-integrated quantities and assume cloud-free conditions, which is a problem over persistent MBL cloud fields. For these reasons, we follow the methodology of Painemal and Zuidema (2011), which uses MODIS cloud product retrievals (Platnick et al. 2003) to calculate the cloud droplet concentration N_c (cm^{-3}). We make the assumption that the number of cloud droplets can be considered a proxy for the CCN concentration, and furthermore assume that the variability in N_c is covariant to that of the CCN concentration (Hudson et al. 2009, 2010). MODIS-effective radius (r_e, here in units of cm rather than μm) and optical thickness (τ) products are combined to estimate N_c:

$$N_c = \Gamma^{1/2} \frac{10^{1/2}}{4\pi\rho_w^{1/2} k} \frac{\tau^{1/2}}{r_e^{5/2}}, \tag{1}$$

which then simplifies to

$$N_c = 1.4067 \times 10^{-6} \frac{\tau^{1/2}}{r_e^{5/2}}. \tag{2}$$

Here ρ_w is the density of water (in $\mathrm{kg\,m}^{-3}$), k is the cubic ratio between the mean volume radius and the effective radius and is assumed to be constant at 0.8, and Γ is the approximate adiabatic liquid water content lapse rate. Further discussion can be found in section 3.4 of Painemal and Zuidema (2011).

Figure 2 shows a time series of CCN concentration ($S = 0.6\%$) from the *RHB*. The period of high CCN concentration early in the simulation is associated with the northwestward movement of a mix of continental and marine aerosol, the concentration of which covaries with MODIS-derived calculations of N_c in Fig. 3. We established our control simulation for the CCN concentration sensitivity tests by taking the average of the CCN concentration over the last 2 days of the simulation ($177\,\mathrm{cm}^{-3}$) and using that value as the initial CCN concentration. Because the synoptic flow is predominantly southerly during the period of interest, the region of high-CCN concentration is advected northward along the continent, leaving the *RHB* lying in a region of more spatially homogeneous CCN, which is confirmed by the CCN time series in Fig. 2. We note that using N_c as a proxy for surface CCN variability is complicated in decoupled boundary layers, which are common far offshore over the southeast Pacific (Bretherton et al. 2010).

c. *Microphysical parameterizations*

The suite of simulations (see Table 1) comprises a number of microphysical parameterizations and CCN

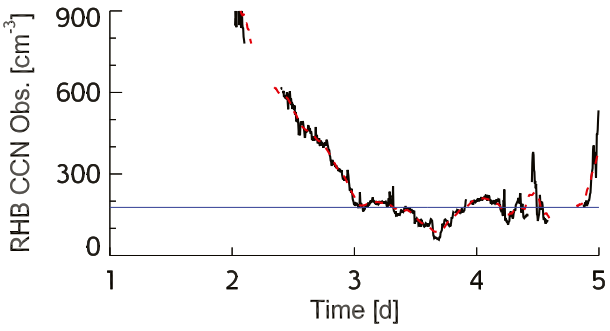

FIG. 2. Observed CCN concentration ($S = 0.6\%$) from the *RHB* during the simulation period. The blue line indicates the calculated mean ($177\,\mathrm{cm}^{-3}$) CCN used to formulate the control CCN concentration initialization. The red line is a moving average of the CCN concentration. Gaps in the data are due to instrumental failure.

concentrations. The operational microphysical parameterization (Rutledge and Hobbs 1983) uses the Kessler warm-rain formulation (Kessler 1969) to establish a baseline control simulation. Additional simulations employ the KK2000 parameterization (Khairoutdinov and Kogan 2000) and a newer parameterization similar to KK2000 but formulated for shallow cumulus clouds (K2013; Kogan 2013). Both KK2000 and K2013 are derived from multivariate nonlinear regressions of droplet spectra obtained from bin-microphysics large-eddy simulations (LES). Table 2 summarizes expressions for the microphysical process rates for each parameterization. The main difference between the operational Kessler parameterization and the KK2000 and K2013 parameterizations is the inclusion of the number concentrations for cloud and precipitation droplets in KK2000 and K2013, which appear in the process-rate equations. In addition, whereas the Kessler parameterization assumes that the precipitation drop size distribution follows a Marshall–Palmer size distribution, the KK2000 and K2013 parameterizations need not make a similar assumption, since all the process rates are statistically derived. The KK2000 and K2013 parameterizations are similarly formulated, but one way they differ is in the exponents of the nonlinear regressions that make up the process rates. In particular, the dependence on N_c in K2013 is approximately double that in the K2000 parameterization, which makes the K2013 parameterization more sensitive to cloud droplet number concentration. Refer to Khairoutdinov and Kogan (2000) and Kogan (2013) for complete descriptions of the two parameterizations. We note that all the KK2000 and K2013 simulations (except for the K2013–N.P. run described below, where cloud-processing of aerosol is turned off) are fully interactive in that they allow for coalescence processing of droplets, which then feeds back upon the CCN field.

In addition to testing the baseline configurations of the KK2000 and K2013 parameterizations, we perform three additional suites of simulations:

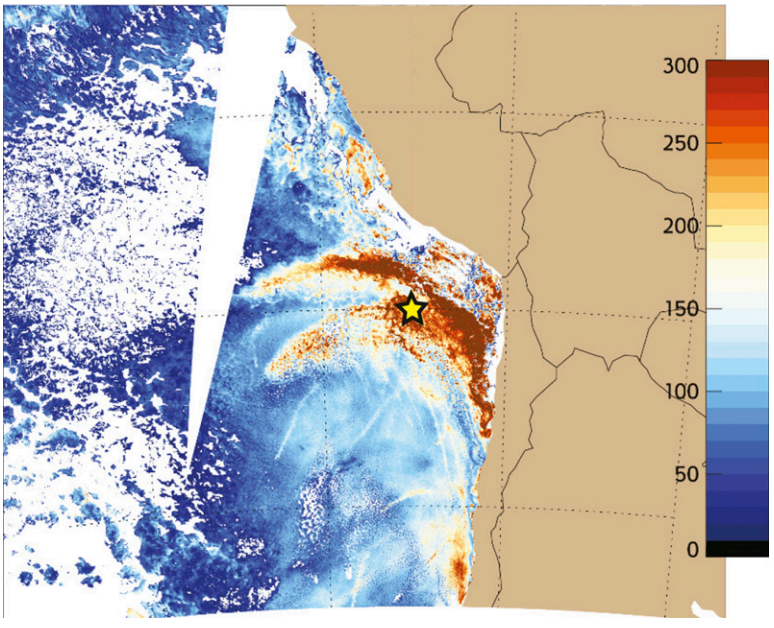

FIG. 3. Plots of droplet concentration N_c calculated from MODIS cloud product effective radius and optical thickness following Painemal and Zuidema (2011) at 1-km resolution for DOY 317 at 1510 UTC. The yellow star indicates the approximate position of the *RHB*. Linear features in the calculated N_c product are ship tracks.

TABLE 1. List of runs completed with COAMPS. Implemented parameterizations and their variations are listed with the varying CCN concentrations used to initialize COAMPS. The Kessler parameterization does not include a droplet or CCN concentration dependence and therefore is considered separately from the rest of the parameterizations.

Parameterization	CCN concentration (cm^{-3})
Kessler	—
KK2000	90
K2013	177
K2013–No S.C.	290
KK2000–threshold	340
K2013–N.P.	700

- The K2013 parameterization also includes a term that represents the self-collection of precipitation droplets that KK2000 does not incorporate. To test the importance of including this self-collection term in a mesoscale model setting, we perform a suite of simulations of K2013 omitting this self-collection (S.C.) term ("K2013–No S.C.").
- Previous research has hinted that the KK2000 parameterization may overestimate autoconversion for high droplet concentrations (Wood 2005). Mechem and Kogan (2008) addressed this issue through the addition of the critical droplet radius threshold of Liu and Daum (2004) to the KK2000 autoconversion rate. We include this formulation as an additional suite of simulations ("KK2000–threshold").
- In our final suite of simulations, the coalescence processing of cloud droplets due to autoconversion and accretion ("K2013–N.P.") is switched off. In contrast to the other KK2000 and K2013 simulations that account for cloud-processing of CCN, this simulation effectively holds $N_{CCN} + N_c$ constant. This was not one of our original simulation suites but is conducted in order to address the overestimation of precipitation by all of our simulations, which we will discuss below.

The sensitivity of the parameterizations to CCN concentration is evaluated by initializing the model with five different CCN concentrations. All simulations assume that the initial CCN field is spatially homogeneous. The control simulation uses a CCN concentration of $177\,cm^{-3}$, as described above. Three additional simulations are initialized with concentrations that are multiples of the control simulation: 90, 340, and $700\,cm^{-3}$. Each of these initializations is chosen as being approximately half, double, and 4 times the control simulation CCN initialization. An additional simulation with a CCN concentration of $290\,cm^{-3}$ conforms to the default oceanic CCN concentration in COAMPS. The combination of multiple parameterizations and CCN values constitute 26 simulations in total.

3. Results

Here we present simulation results and compare them with *RHB* observations. We also evaluate the internal consistency of model microphysical processes by exploring how well simulated cloud properties adhere to observationally derived scalings for precipitation rate and coalescence processing.

a. *Simulation summary and comparison with* RHB *observations*

Figure 4 shows time–height contour plots of cloud water mixing ratio q_c, rainwater mixing ratio q_r, and liquid water potential temperature θ_l for each parameterization on the inner mesh (3 km) of the simulations using the baseline CCN concentration ($177\,cm^{-3}$). The observed MBL depth derived from the *RHB* soundings is overlaid on the figures. MBL depth from both the soundings and simulation output was calculated following the method of de Szoeke et al. (2012), which assigns the MBL depth to the level of a relative minimum absolute temperature in each column. To prevent erroneous MBL depths, we only considered temperatures in the lower 23 sigma levels (about 1750 m). Rahn and Garreaud (2010a) used a similar method in their study to calculate MBL depth.

TABLE 2. Details of the equations that compose each parameterization used in the study. The operational version of COAMPS uses the Kessler (1969) warm-rain parameterization. The factor $G(T, p)$ in the KK2000 and K2013 parameterizations represents the coefficient in the condensational growth equation and is equivalent to Eq. (7.40) in Rogers and Yau (1989). Here C_p is a constant of proportionality defined as $(4\pi\rho_w/3\rho_a)^{2/3}$.

	Kessler	KK2000	K2013
Accretion	$6.96\times10^{-4}EN_0^{1/8}q_cq_r^{7/8}$	$67(q_cq_r)^{1.15}$	$8.53q_c^{1.05}q_r^{0.98}$
Autoconversion	$k_1(q_c-a)$ $k_1=10^{-3}\,s^{-1}$, $0.5<a<1.0\,g\,kg^{-1}$	$1350.0q_c^{2.47}N_c^{-1.79}$	$(7.98\times10^{10})q_c^{4.22}N_c^{-3.01}$
Fall speed	$V=-38.3N_0^{-1/8}q_r^{1/8}$	$V_{N_r}=0.007r_{vr}-0.1$ $V_{q_r}=0.012r_{vr}-0.2$	$V_{N_r}=0.385r_{vr}+5.76$ $V_{q_r}=2.4r_{vr}-62.0$
Evaporation	$1.93\times10^{-6}N_0^{7/20}q_cq_r^{13/20}$	$3C_{evap}G(T,p)C_pq_r^{1/3}N_r^{2/3}S$	$3C_rG(T,p)SC_pq_r^{1/3}N_r^{2/3}$
Self-collection	—	—	$205q_r^{1.55}N_r^{0.60}$

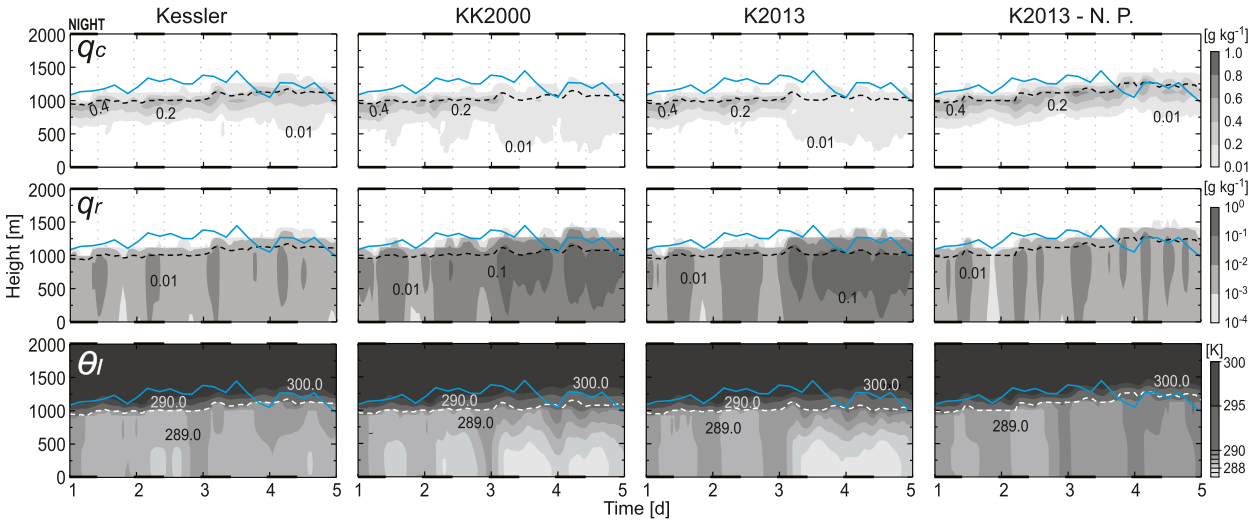

FIG. 4. Time–height cross sections of q_c, q_r, and θ_l from the inner 3-km mesh for each parameterization and the control CCN concentration (CCN = 177 cm^{-3}). Dotted vertical lines separate periods of day and night. The blue line indicates the observed MBL depth, and the dashed lines denote MBL depth calculated from the simulations.

All simulations exhibit a persistent layer of stratocumulus with varying amounts of drizzle (indicated by q_r) falling below cloud base. The most obvious differences across the simulations stem from differences in the amount of precipitation produced. The precipitation structure q_r in KK2000 and K2013 simulations are both similar, and both simulations display a profound stratification (stabilization) of the boundary layer, particularly starting on day 3. This stratification is associated with the presence of substantial precipitation and a reduction of cloud liquid water q_c. The stabilization of the boundary layer is the result of the warming of the upper boundary layer and the cooling of the surface layer. Warming of the cloud layer arises from the drizzle-induced asymmetry in the MBL circulation (i.e., the potential buoyancy arguments of Stevens et al. 1998), and cooling in the subcloud layer is simply a result of evaporating drizzle. The Kessler simulation drizzles strongly but does not produce the same degree of stratification in the boundary layer, a result we attribute to overly large precipitation fall speeds (and hence weaker evaporation) associated with the assumed negative exponential precipitation drop size distribution. In most respects, however, the Kessler parameterization performs admirably given its simplicity.

The rapid change in the model fields during day 3 (enhanced precipitation, greatly reduced cloud water, and increased stability) is coincident with model fields that depart substantially from observations (Fig. 5) and constitutes simple model forecast error. However, we hypothesize that this transition behavior arises from our lack of CCN source in the simulations, whereby precipitation efficiency steadily increases day after day, as droplet concentration decreases (<10 cm^{-3} in the 177 cm^{-3} simulations) and is never replenished. In simulations with greater initial values of CCN, the decrease of droplet concentration is not as dramatic, because of the smaller values of coalescence scavenging associated with weaker precipitation. The K2013–N.P. simulation that neglects coalescence processing exhibits weaker precipitation and maintains a more robust cloud layer over the entire course of the simulation. Weaker precipitation reduces the evaporative cooling over the subcloud layer, and the stabilization is less than in the KK2000 and K2013 simulations.

The model exhibits a diurnal cycle of precipitation and θ_l (Fig. 4), particularly evident early in the simulation. The timing of the precipitation onset is consistently just after local sunset, which is roughly consistent with observations over the western portion of the VOCALS domain in Burleyson et al. (2013). The K2013–N.P. simulation exhibits the strongest diurnal cycle in cloud water and precipitation.

Figure 5 shows time series of simulated LWP, MBL depth, and precipitation rate, all compared with *RHB* observations for the control simulation suite (all the 177 cm^{-3} runs). Time-averaged LWP, MBL depth, and precipitation rate are given in Table 3 and visualized in Fig. 6 for easier comparison across microphysical parameterizations and CCN initializations. Both Figs. 5 and 6 indicate that all simulations underestimate LWP relative to that observed by the *RHB*. The simulation-mean LWP increases as the CCN concentration increases, which indicates suppression of precipitation by large CCN concentrations. The time series show that

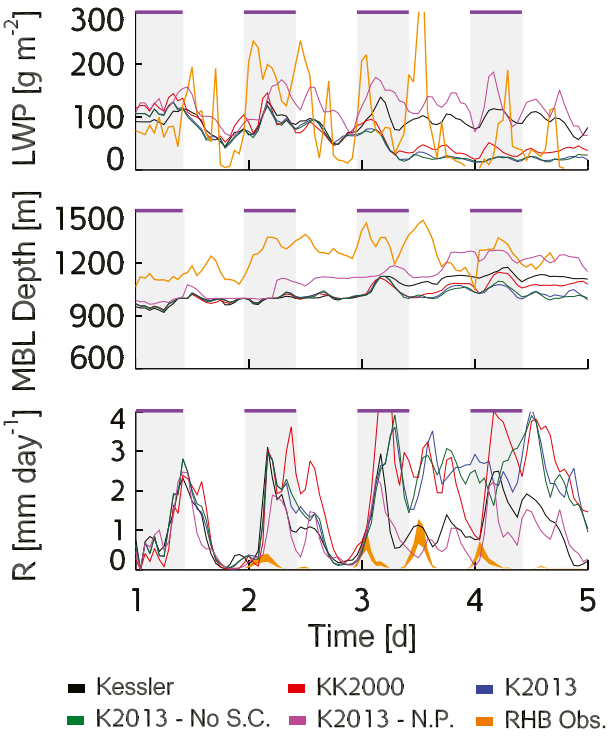

FIG. 5. Time series of hourly LWP, MBL, and R from the inner nest for each simulation using the control CCN concentration (CCN = 177 cm^{-3}), along with observations from *RHB*. The gray bars topped by purple lines indicate nighttime. The observed precipitation rate R is bound by rates corresponding to a reflectivity range of ± 2 dBZ corresponding to uncertainties in the radar calibration.

larger peaks in model LWP tend to occur coincidentally with the strongest precipitation rates overnight and particularly several hours after sunset. This precipitation behavior contrasts with the findings of Burleyson et al. (2013) over the eastern portion of the VOCALS domain, which show a maximum of precipitation closer to sunrise. Burleyson et al. (2013) also found that drizzle was present during daytime hours, which our simulations show as well. One source of discrepancy between the observed and simulated LWP values is due to the *RHB* LWP being a point measurement from the ship, whereas the model LWP is averaged over the *RHB* radar volume. Except for the KK2000–threshold simulation, the largest LWP values come from the K2013–N.P. simulations and are associated with weaker precipitation rates, suggesting that precipitation and dynamic feedbacks associated with precipitation is this case can strongly modulate cloud water content.

The middle panel of Fig. 5 shows the hourly averaged MBL depth for the simulation and, as for LWP, exhibits the same overall model underestimation relative to observations. Underestimation of MBL depth is a persistent problem in both mesoscale and climate models (Wyant et al. 2010; Wang et al. 2011; Wyant et al. 2015). Previous research has demonstrated that MBL depth is affected by CCN concentration through influencing precipitation magnitude and the subsequent stabilization of the MBL, which leads to a reduction of cloud-top entrainment (Mechem et al. 2006). Combined, these effects result in a shallower boundary layer, but more generally the cloud responses can be a nonlinear combination of influences from surface fluxes, radiation, and entrainment. Uncertainties in subsidence rate can also lead to errors in MBL depth, but the results of Wood et al. (2009) suggest that the subsidence imposed by large-scale models over the VOCALS region is largely believable. Ideally, the subsidence rate is unbiased and contains only random errors, but we are unaware of any study that has formally evaluated this over the marine stratocumulus regions. Because of smaller precipitation rates throughout the majority of the simulation period, the K2013–N.P. simulations exhibit a higher MBL depth than the other simulations. Of all the simulations, the K2013–N.P. simulations have the lowest rain rates, exhibit the most pronounced diurnal cycle, and best match the observations.

Nearly all simulations drastically overestimate precipitation rate relative to the *RHB* observations (Fig. 5), but the exact reason is not clear. Some of the discrepancy may be attributable to slight differences in what the two quantities represent. The simulation precipitation values are evaluated at the surface, whereas the radar-derived precipitation rates roughly represent a mean over the subcloud layer (since the precipitation rate actually applies to a radar beam of finite width, rather than being defined exactly at some particular level). We have estimated that subcloud precipitation rate in the simulations is, on average, ~30% greater than the surface precipitation rate. This difference in definition, however, is insufficient to explain the large departures from the *RHB* radar-derived precipitation rates. The bulk of the difference is due to coalescence processing, which ultimately reduces the CCN, leading to increased precipitation efficiency. This effect is why the K2013–N.P. precipitation rates, which hold $N_{CCN} + N_c$ constant, are substantially smaller than the other simulations (see Table 3). We speculate also that some of the differences are due to the inability of a 3-km horizontal grid to adequately resolve organized mesoscale precipitation structures (Comstock et al. 2005).

In addition to the parameterization suite shown in Fig. 5, Table 3 and Fig. 6 include results from an additional simulation series, where the critical radius threshold from Liu and Daum (2004), as simplified by Wood (2005), is imposed on the autoconversion term from KK2000 following Mechem and Kogan (2008). The motivation for

TABLE 3. Simulation means evaluated over the *RHB* radar volume for LWP ($g\,m^{-2}$), MBL depth (m), and precipitation rate ($mm\,day^{-1}$). The KK2000–threshold run includes the addition of a critical radius threshold for autoconversion following Liu and Daum (2004), and K2013–N.P. represents the simulation that removes the coalescence processing due to autoconversion and accretion. The observational means are given as a single value covering the range of CCN values observed during VOCALS. The Kessler mean is given as a single value because of its lack of droplet concentration dependence. Uncertainty on the microwave radiometer retrieval is ~20% (Hogg et al. 1983). Uncertainty on the observational estimate of z_i depends on the radar range gate spacing, which in this case is 25 m (de Szoeke et al. 2012). Given a ±2-dBZ uncertainty in the radar reflectivity, we conservatively estimate the *RHB* precipitation rate uncertainty to be $0.074 \pm 0.079\,mm\,day^{-1}$.

	CCN concentration	*RHB*	Kessler	KK2000	K2013	K2013–No S.C.	KK2000–threshold	K2013–N.P.
LWP	90			39.62	29.90	26.66	188.30	85.16
	177			62.37	53.57	52.81	191.81	104.48
	290	92.35	80.11	83.71	80.96	79.39	187.77	120.64
	340			89.79	91.05	90.25	193.78	126.41
	700			122.85	123.05	126.45	194.75	137.56
z_i	90			1022.95	949.57	966.47	1090.09	1053.85
	177			984.52	971.94	970.44	1090.03	1059.08
	290	1217.27	999.17	1002.02	1003.98	1003.46	1080.26	1064.12
	340			1042.74	1043.74	1009.96	1089.62	1067.42
	700			1073.37	1022.70	1069.56	1090.15	1071.49
R	90			1.923	1.857	1.867	0.069	0.935
	177			1.518	1.374	1.378	0.0246	0.682
	290	0.074	0.859	0.964	0.80	0.842	0.015	0.501
	340			1.104	0.864	0.699	0.0082	0.483
	700			0.587	0.353	0.505	0.0044	0.376

these simulations is to address the overestimation of precipitation in a physically meaningful way. Imposing this threshold on the autoconversion process suppresses the precipitation rates for simulations initialized with higher CCN concentrations. The rain rates in the KK2000–threshold simulations approach the observed rain rates (Table 3 and Fig. 6). LWP and MBL depth nevertheless remain anomalously high (low) relative to the *RHB* observations. This result suggests that although the critical radius threshold reduces precipitation, this approach may not be physically plausible. For this reason, we do not include the simulation in our further discussions.

To investigate the statistical variability of the model output we constructed normalized probability density functions (PDFs) of LWP, MBL depth, and R from three different initial CCN values, along with the *RHB* observations (see Fig. 7). The PDFs are calculated over a radius of 60 km corresponding to the sampling area of the *RHB* C-band radar (centered at 20°S, 75°W). The PDF of the Kessler LWP differs most from the observational PDF and includes none of the larger LWP values in the tail of the observed PDF. As CCN concentration increases, the PDFs of LWP for the tested parameterizations shift from a negative exponential distribution to a more Gaussian distribution, yet they still differ substantially from the observed LWP PDF. The PDF of LWP from the K2013–N.P. simulation does not exhibit the negative exponential distribution as do the other simulations, but rather remains relatively Gaussian across all CCN concentrations and widens as the CCN concentration increases.

The narrowness and similarity of the MBL depth distributions in the CCN = 177 and $340\,cm^{-3}$ simulations suggest that CCN plays little role in modulating MBL depth (Fig. 7). Only for the cleanest case (CCN = $90\,cm^{-3}$) do modest differences in MBL depth begin to appear. When considering MBL depth variability, we acknowledge the possibility that COAMPS may not be adequately representing the diurnal "upsidence wave" described in Garreaud and Muñoz (2004), although assessing how well COAMPS represents the upsidence wave is beyond the scope of this study. Furthermore, we hypothesize that the coarse horizontal grid spacing of our simulations results in a lack of resolved internal mesoscale variability, including many aspects of open and closed cells.

The PDFs of both the model and observed precipitation rates are negative exponential distributions. The model PDFs do not appear to differ much across the different CCN concentrations, but the KK2000 simulations have the best agreement with the shape of the observational precipitation rate PDF. All simulations include instances of precipitation rates larger than those observed ($>1.2\,mm\,day^{-1}$).

Figure 8 casts the model output from all simulations (except the KK2000–threshold) in N_c–LWP parameter space. The data points are color coded both by parameterization (Fig. 8a) and by the rain rate (Fig. 8b). For each parameterization we include simulation mean N_c

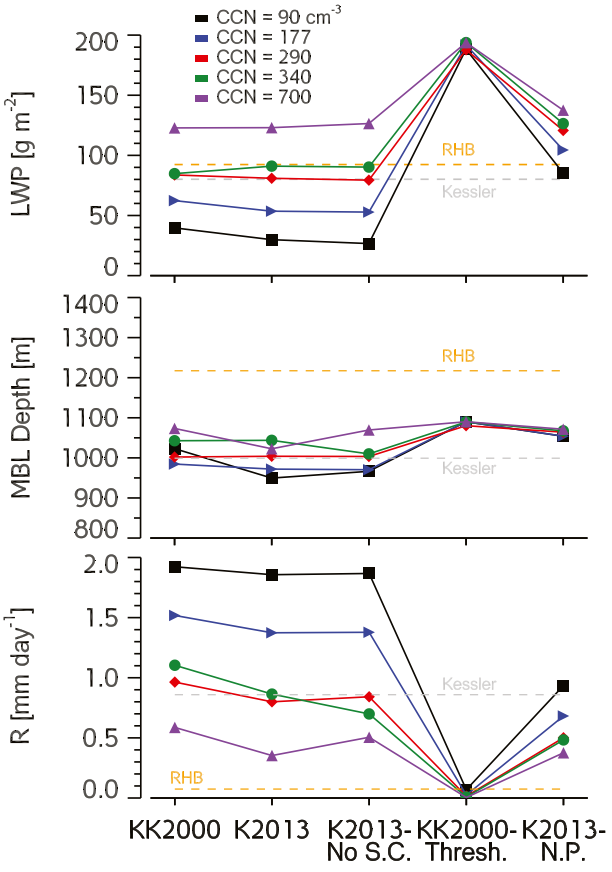

FIG. 6. Simulation means of LWP, MBL depth, and R for all parameterizations and all CCN initializations. The Kessler simulation mean is indicated by the horizontal dashed gray line labeled "Kessler." The observations from the *RHB* are represented by the horizontal dashed orange line.

and LWP values that encompass all sensitivity simulations through time. Since the Kessler microphysics does not employ a prognostic N_c, we include a band corresponding to the range of hourly domain-averaged LWP values for the Kessler simulation in Fig. 8b in order to assess the performance of the Kessler parameterization relative to the other parameterizations. The distribution of data within parameter space is consistent with higher precipitation rates accompanying lower CCN concentrations and larger LWP, and smaller precipitation rates accompanying with higher CCN concentrations. Although it is well known that the highest rain rates will occur in cleaner cases, the model exhibits a sharp increase in precipitation range at $N_c \approx 30\,\mathrm{cm}^{-3}$, where precipitation rates are nearly $1\,\mathrm{mm\,day}^{-1}$ higher than those for $N_c > 30\,\mathrm{cm}^{-3}$. Furthermore, variability in LWP for a given cloud droplet concentration increases as the CCN concentration increases. We speculate that the low mean values of N_c relative to the observations may be the result of precipitation scavenging of droplets and the lack of a suitable source of CCN in the model (Mechem et al. 2006). The mean N_c of our results from the K2013–N.P. simulation support this hypothesis.

b. *Scalings for precipitation rate and coalescence scavenging*

Without regular data analysis update cycles, over the course of a 4-day simulation, we expect the simulation results at any given point and time will begin to differ from observations. Letting the model run unconstrained by data assimilation cycles, forced only by SST and at the domain boundaries, gives substantial insight into intrinsic model behavior. Instead of insisting on point-by-point comparisons between model and observation, here we explore how well the simulation results adhere to observationally and theoretically derived scalings, which we interpret as a measure of microphysical consistency in the model. In this section, we use the term "microphysically consistent" to indicate that the microphysical aspects of the model seem to be internally in agreement (consistent), suggesting that model error likely has sources other than the model microphysics. Our analysis is similar to the methodology of Geoffroy et al. (2008), where we compare the model output to scalings we assume, broadly speaking, to be true.

Figure 9 shows simulation precipitation rates plotted as a function of the scalings from Comstock et al. (2004) and van Zanten et al. (2005), using simulation values of mean cloud thickness, LWP, and N_c, evaluated over the *RHB* radar volume. The adapted equation from Comstock et al. (2004) is

$$R = 0.3744(\mathrm{LWP}/N_c)^{1.75}, \tag{3}$$

where R is the precipitation rate (in $\mathrm{mm\,day}^{-1}$), LWP (units of $\mathrm{g\,cm}^{-2}$), and N_c (units of cm^{-3}). The precipitation scaling from van Zanten et al. (2005) depends on the cloud thickness, h, instead of LWP and has the following form:

$$R = 2 \times 10^{-6}(h^3/N_c). \tag{4}$$

Here the units for R and N_c are the same as in Eq. (3), and h has units of meters. These scalings were also created for the *RHB* observations and are shown in the right-hand column of Fig. 9. Our analyses here do not include results from the Kessler simulation because the Kessler formulation does not include the dependence on droplet concentration present in both of these scalings.

The observational scalings hold relatively well for the model output. The van Zanten et al. (2005) scaling is based on flight-mean values of h, N_c, and R;

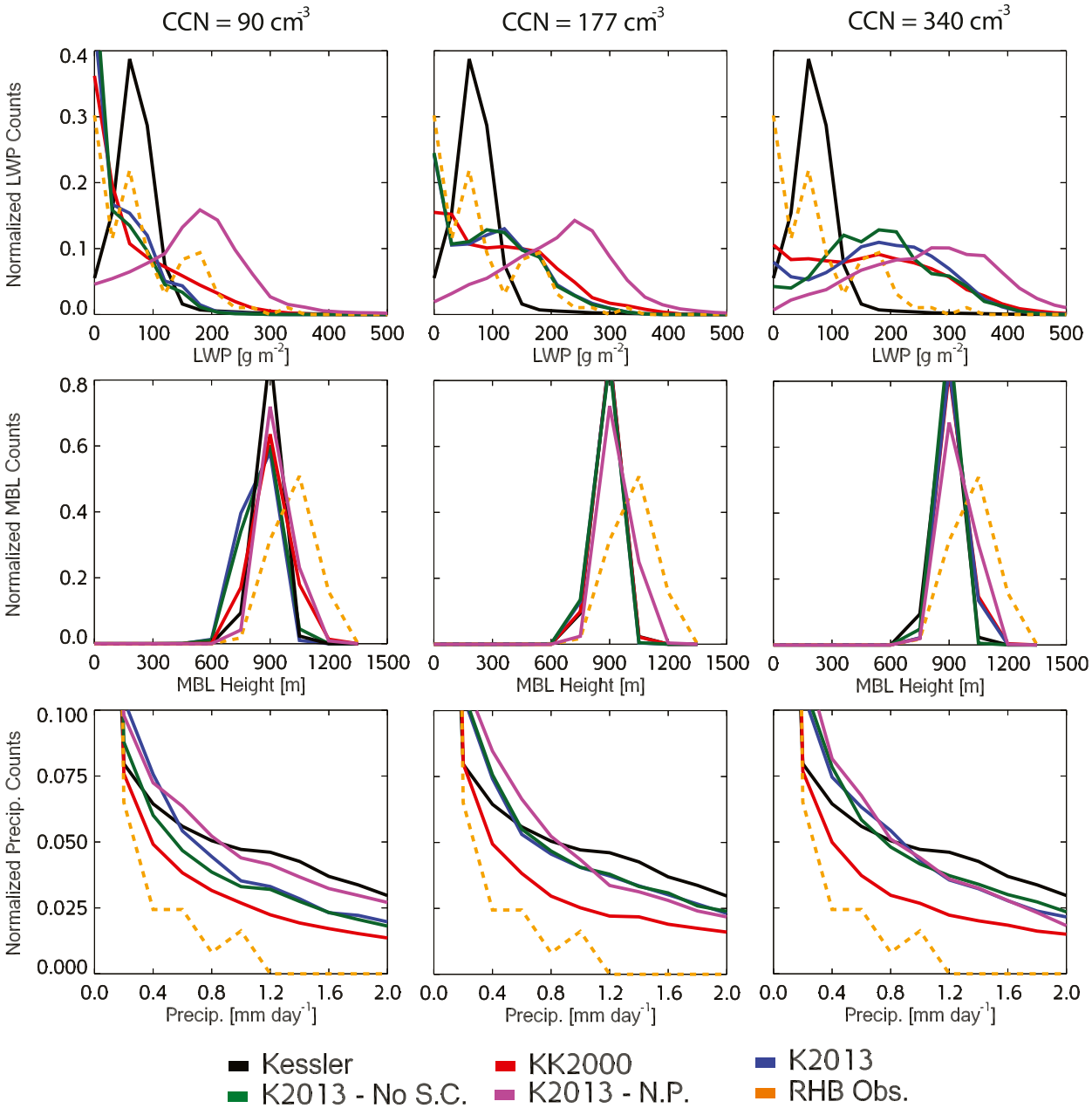

FIG. 7. Probability density functions calculated over the volume of the C-band radar (60-km radius) on board the *RHB* for LWP, MBL, and R for the control CCN concentration (CCN = 177 cm^{-3}), as well as concentrations half and double the control concentration. PDFs of the observational quantities are given by the dashed orange lines.

nevertheless, instantaneous values of these quantities tend to cluster near the h^3/N_c line in Fig. 9. The model output scalings show a wider range of precipitation rates than the observations in Comstock et al. (2004, their Fig. 10) and van Zanten et al. (2005, their Fig. 7a), at least partially because of our simulations overestimating the precipitation rate, which we previously addressed. Geoffroy et al. (2008) evaluated these scalings for LES output and found a similar level of agreement. The majority of the rain rates for both scaling studies lie between 0.1 and 1.0 mm day^{-1}. The scaling values for Comstock et al. (2004) lie between $(\mathrm{LWP}/N_c)^{1.75} = 0.5$ and 100.0 g m^{-2} cm^3 and the scaling values for the van Zanten et al. (2005) study lie between $h^3/N_c = 10^5$ and 10^7 m^3 cm^3. Our results from the K2013–N.P. simulation also follow the scalings with the rain rates being substantially lower than the other simulations as discussed above.

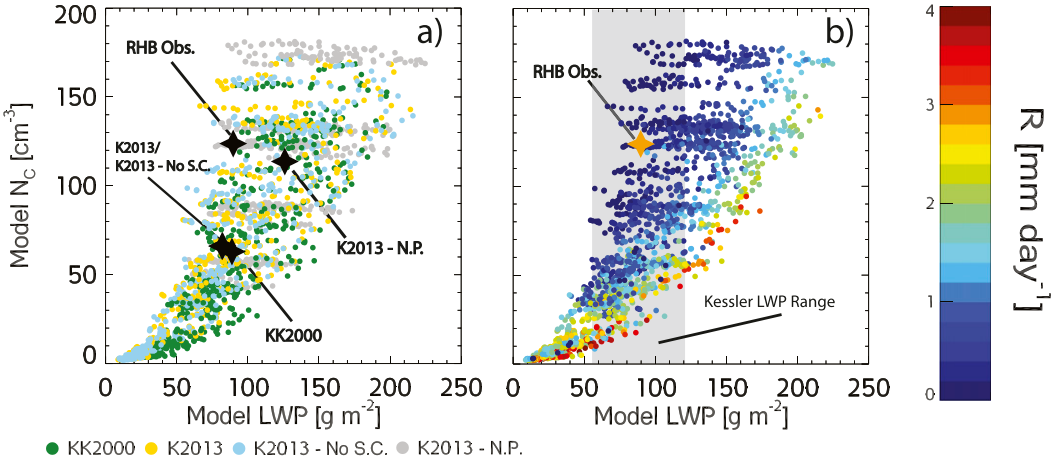

FIG. 8. Scatterplots of N_c vs LWP from the inner nest for all parameterizations and all CCN concentrations. The distribution of points stratified by (left) parameterization and (right) precipitation rate. The mean N_c and LWP for each parameterization are plotted in the (left). In lieu of scatter points for the Kessler simulations, we use the gray bands to indicate the range of hourly domain-averaged LWP values from the Kessler simulation.

Figures 9a and 9c contain a scale break at approximately $(\mathrm{LWP}/N_c)^{1.75} = 5.0$ and $h^3/N_c = 5.0 \times 10^5$, respectively, where the slope of the cluster of points changes substantially. This scale-break behavior is not present in the LES scalings of (Geoffroy et al. 2008) and may derive from two different sources. The first arises from a possible discrepancy among where the precipitation rates are evaluated. The observational scalings were developed using cloud-based rain rates, whereas the model output (because it is an operational model) provides only surface precipitation, and the radar precipitation rates are representative of the subcloud layer as a whole. We hypothesize that using cloud base instead of surface rain rates would increase the rain rates for the lower $(\mathrm{LWP}/N_c)^{1.75}$ and h^3/N_c scalings because the drizzle rates are highest at cloud base, moving those points upward on the figure (toward higher R).

We evaluated the sensitivity of the scalings to the vertical level where simulated precipitation is sampled. We calculated the cloud-base precipitation rates and found that they are, on average, ~60% greater than the surface precipitation. Because the radar precipitation rates are characteristic of the subcloud layer, this ~60% value corresponds to an increase of ~30%, representative of the subcloud layer. The modest ~30% bias in precipitation rate is within the realm of observational uncertainty from the radar and the Z–R relationship, and the precipitation and coalescence scavenging scalings (not shown) are not noticeably different when employing either surface or subcloud-layer precipitation rates.

A second possible explanation for the scale break stems from a simple water budget constraint. We have included a purple line at $R = 2.6\,\mathrm{mm\,day^{-1}}$ on Fig. 9 that corresponds to the mean latent heat flux for all simulations ($76.86\,\mathrm{W\,m^{-2}}$), with the idea that surface moisture flux is a limiting factor for mean precipitation. If true, this latent heat flux limiting behavior suggests that the scale break is not entirely physical but is at least in part an artifact of the model's tendency to overproduce precipitation. Geoffroy et al. (2008) also found significant overestimation of precipitation rates in their analysis of LES output. The K2013–N.P. simulation does not exhibit the scale break that the other simulations do, most likely because the precipitation rates are not as high as they are in the other simulations and thus need not be bound by the surface moisture flux.

In addition to scalings for precipitation rate, we also explore scalings for coalescence processing, which represents the depletion rate of cloud droplets from coalescence. Figure 10 shows coalescence processing rates from all simulations, plotted as a function of the product of N_c and R, the dominant term in two scalings found in the literature (Mechem et al. 2006; Wood 2006). Figure 10 replicates the scalings in two specific studies, each with their own regression equations for CCN depletion. Wood (2006) developed a theoretically based expression for coalescence processing, given as

$$D = 120(N_c R). \tag{5}$$

Mechem et al. (2006) found a formulation based on highly idealized COAMPS simulations, given as

$$D = 69.4(N_c R)^{0.668}. \tag{6}$$

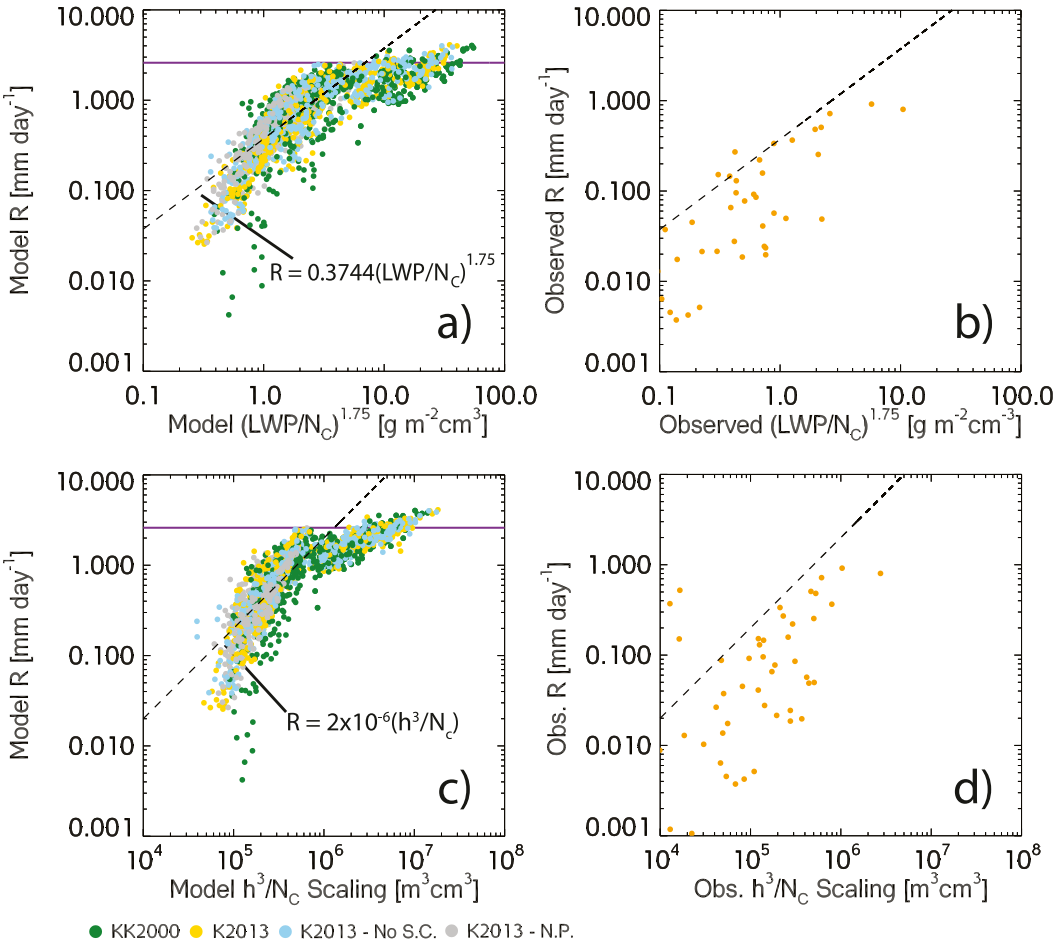

FIG. 9. Precipitation scalings for the inner nest and observations from *RHB*. (a),(b) The scalings follow Comstock et al. (2004), and (c),(d) scalings follow van Zanten et al. (2005). The equations for each scaling have been adapted from both previous studies to the units used in this study. The solid purple line indicates a rain rate calculated from the equivalent mean latent heat flux from all simulations.

In both equations, N_c is the number concentration of cloud droplets (in cm^{-3}), R is the precipitation rate (in $\mathrm{mm\,day}^{-1}$), and D is the depletion rate of cloud droplets (in $\mathrm{cm}^{-3}\,\mathrm{day}^{-1}$). From Fig. 10, it is clear that the KK2000 parameterization holds best to both previous studies' depletion scalings across the range of N_c and R values based on how closely the KK2000 data points cluster narrowly around the scaling regression lines. The somewhat wider spread of data from the K2013 and K2013–No S.C. runs nevertheless reasonably follow the coalescence scavenging scalings found in Wood (2006) and Mechem et al. (2006). The results from the K2013–N.P. simulation lie very near the scaling line from Wood (2006) and do not exhibit the same spread as the other simulations, most likely because the total particle concentration ($N_c + N_{\mathrm{CCN}}$) is constrained. A similar figure for the *RHB* observations is not available, because the N_c depletion rate was not observationally available from the VOCALS-REx datasets.

Figure 11 shows the previous scalings but over the outer nest (with 27-km grid spacing). The most obvious results from evaluating scalings on the outer nest are the significantly wider distribution of data points and the complete disagreement with the observational scalings. This suggests that lower-resolution simulations of the cloud marine boundary layer may not remain microphysically consistent and that the results from those simulations are not as robust. The reason for this discrepancy is not clear but may be related to mesoscale organization that is resolved on the 3-km grid but not on the 9-km mesh (e.g., Mechem and Kogan 2003).

Figure 12 shows the same scalings but for the middle (9 km) nest. These results confirm that model horizontal resolution remains acutely important to microphysical consistency. The spread of the data in the precipitation

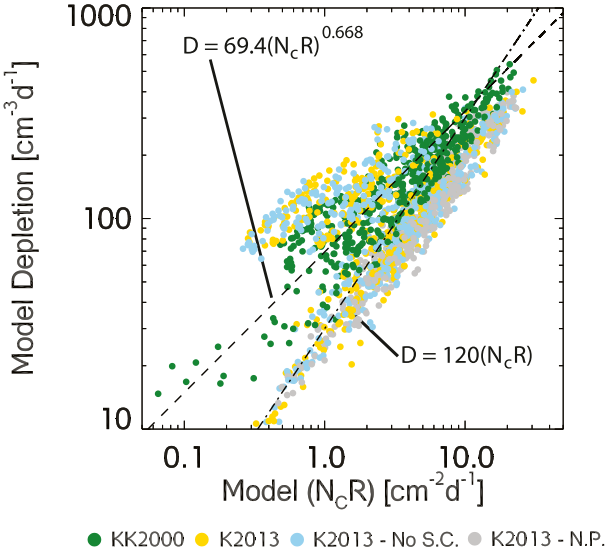

FIG. 10. Scatterplot of coalescence processing as a function of N_cR. Dashed black lines represent the coalescence processing scalings of Wood (2006) and Mechem et al. (2006).

scalings show a similar behavior to the finest mesh simulation in Fig. 9, which suggests that the cloud-system behavior on the 9-km grid is microphysically consistent. Coalescence processing rates on both the 27- and 9-km grids adhere to the scalings of Mechem et al. (2006) and Wood (2006).

4. Discussion and conclusions

We have presented the results from a suite of COAMPS simulations to evaluate a number of warm-rain microphysical parameterizations. The simulations are run over the period of 12–16 November 2008 and then compared to multiplatform observations from the VOCALS field campaign. The suite of simulations demonstrates that the K2013 and KK2000 parameterizations behave similarly over the 4-day VOCALS period. This similarity is perhaps unsurprising, given the multivariate nonlinear regression method that forms the basis of both parameterizations (Khairoutdinov and Kogan 2000; Kogan 2013), even though the individual formulations themselves have substantial differences in process rates (see Table 2). The choice of parameterization also only modestly affects the distributions of cloud properties (PDFs of LWP, MBL depth, and R). Figure 5 shows that the simulations begin to diverge substantially from observations only after two full days. We interpret this divergence for the most part as the simple growth of forecast error with time that all numerical weather prediction models exhibit. The overestimate of precipitation is substantially affected by

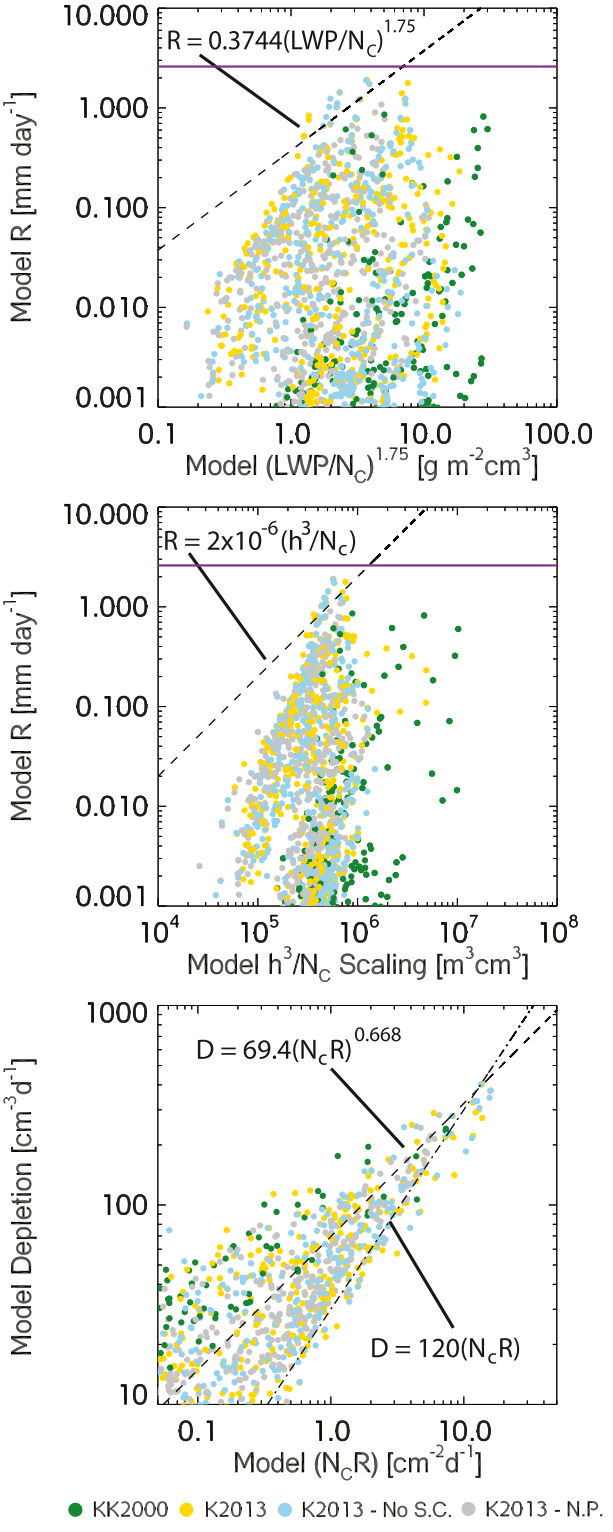

FIG. 11. Scalings from Figs. 9 and 10, but for the outer 27-km nest.

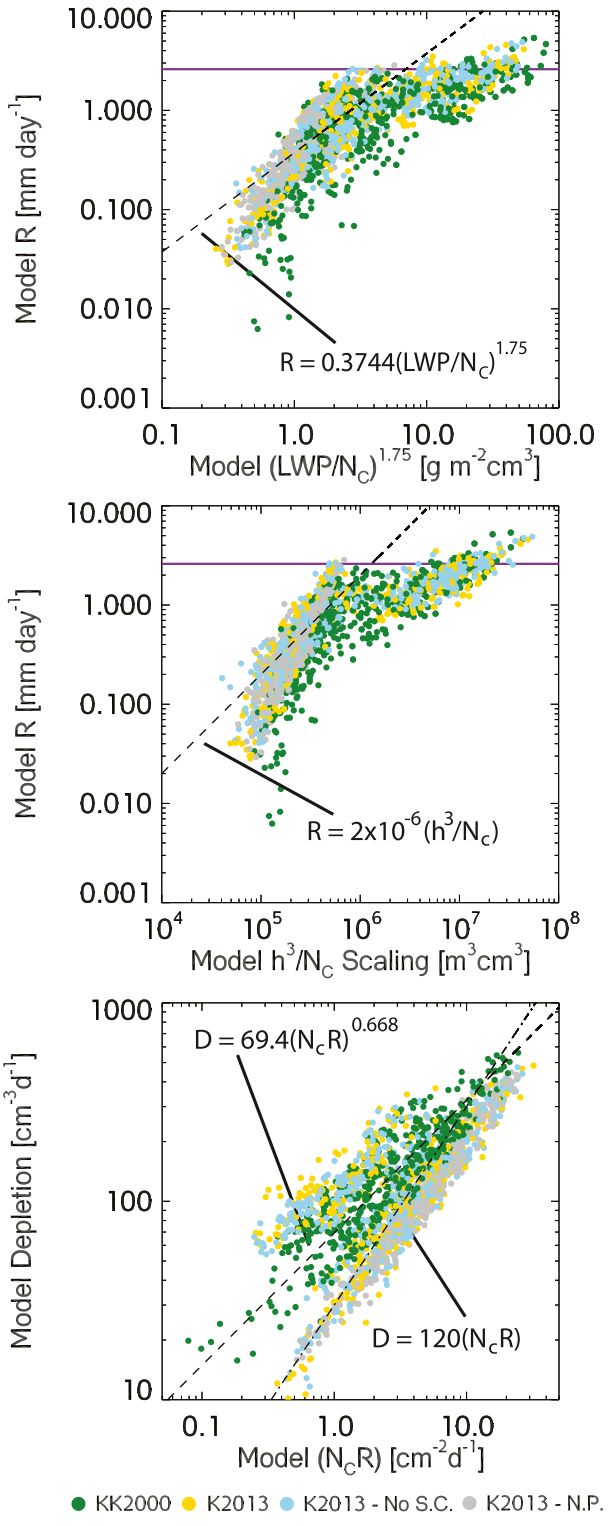

FIG. 12. Scalings from Figs. 9 and 10, but for the middle (second) 9-km nest.

precipitation efficiency increasing over the course of the simulation, since CCN is never replenished. Although we naturally expect precipitation efficiency increases to accompany lower CCN concentrations away from shore, the lack of a CCN source in the model greatly exaggerates this behavior. Some of these errors appear to be reduced when $N_{CCN} + N_c$ is held constant (Fig. 5), suggesting the importance of parameterizing a source term for CCN or imposing a fixed, climatological background CCN concentration.

Although the KK2000 and K2013 parameterizations behave similarly, K2013 shows promise for being the best choice (of the three implemented parameterizations) for primary use in mesoscale models due to its generality and ability to perform in both stratocumulus and trade cumulus cloud regimes (Kogan 2013). While the K2013 autoconversion formulation suggests a much greater dependence on N_c, our simulations do not exhibit this behavior, suggesting that nonlinear behaviors in process rates may not directly translate to differences in MBL cloud-system properties. We also note that the self-collection term in the K2013 simulations makes little difference in cloud properties, at least for this particular VOCALS case.

Nearly all of the simulations differ substantially from the observations (Table 3 and Fig. 6). As always, the horizontal and vertical resolution play an important role in accurately simulating the MBL depth, and with increased computational infrastructure, forecast error associated with resolution can be expected to steadily decrease (Wang et al. 2011; Wyant et al. 2015). The differences in cloud properties between the observations and the simulation suite are greater than the differences among the simulation ensemble, suggesting that the disagreement with observations, both here and in other studies that include mesoscale models (e.g., Wyant et al. 2010; Wang et al. 2011; Wyant et al. 2015), may result more from errors in representing MBL dynamics than those from microphysical processes. At the very least, the shallow bias in simulated MBL depth is a consistent feature across a number of modeling studies.

We find that our simulation results are broadly consistent with observationally derived scalings for precipitation rate and coalescence scavenging, a finding we interpret to be indicative of microphysical consistency. These findings largely parallel those of Geoffroy et al. (2008), whose LES simulations closely resemble the precipitation rate scalings evaluated from three different observational studies. In order for our mesoscale model simulations to exhibit microphysical consistency, the models must be run at relatively high resolutions (to be safe, approximately a 10-km grid spacing or finer). We note that the microphysical scalings evaluated in

this work apply only to marine stratocumulus-topped boundary layers over the southeast Pacific VOCALS region. We have not evaluated the applicability of the scalings and parameterization behavior over the other oceanic stratocumulus regions, but hopefully the results are broadly applicable. Exploring these microphysical scalings in other marine boundary layer cloud regimes is ripe for future study.

Our results suggest the following recommendations to follow when running mesoscale model simulations of marine stratocumulus. First, the horizontal grid spacing should be no coarser than 10 km to ensure microphysical consistency. Our results indicate that cloud properties (LWP, MBL depth, and R) degrade substantially somewhere in this range. If computational resources or time can be afforded, grid spacings smaller than 10 km are preferable, of course. Second, based on its generality, we suggest the use of the Kogan (2013) warm-rain microphysics parameterization because of its applicability to both stratocumulus cloud sheets and trade cumulus regimes. However, the KK2000 parameterization performs equally as well over the VOCALS period studied here. Simulations in the trade cumulus regime may better reap the advantages of the K2013 parameterization. We speculate that including other methods of parameterizing subgrid-scale microphysical processes, such as the PDF formulation suggested in Kogan and Mechem (2014) may improve model performance further. Furthermore, because of the difference in scaling behavior across the different grid sizes, efforts to make the physical processes in model ''scale aware'' should be pursued (Boutle et al. 2014b).

Acknowledgments. Author K. Nelson acknowledges ONR support for his M.S., of which this article is the final product. We are grateful to three anonymous reviewers, whose comments helped improve the science and presentation of the manuscript. We appreciate the helpful and patient guidance of Shouping Wang in formulating our COAMPS experimental design. The authors thank Simon de Szoeke (estimates of cloud-base and inversion heights, and surface observations), Sandra Yuter (radar precipitation estimates), and Paquita Zuidema (LWP retrievals) for the observational VOCALS-REx datasets from the NOAA R/V *Ronald H. Brown* used in this research. Thanks to Dave Rahn and Donna Tucker for constructive comments on the manuscript. Dave Covert supplied CCN observations. Beth Tully improved the presentation of several of the figures. Y. Kogan acknowledges ONR and CIMMS support. This research was supported by Office of Naval Research Awards N00014-11-1-0518 (Mechem) and N00014-11-10439 (Kogan).

REFERENCES

Albrecht, B. A., C. S. Bretherton, D. Johnson, W. H. Schubert, and A. S. Frisch, 1995: The Atlantic Statocumulus Experiment—ASTEX. *Bull. Amer. Meteor. Soc.*, **76**, 889–904, doi:10.1175/1520-0477(1995)076<0889:TASTE>2.0.CO;2.

Baker, M. B., 1993: Variability in concentrations of cloud condensation nuclei in the marine cloud-topped boundary layer. *Tellus*, **45B**, 458–472, doi:10.1034/j.1600-0889.45.issue5.1.x.

Bony, S., and J.-L. Dufresne, 2005: Marine boundary layer clouds at the heart of tropical cloud feedback uncertainties in climate models. *Geophys. Res. Lett.*, **32**, L20806, doi:10.1029/2005GL023851.

Boutle, I., and S. Abel, 2012: Microphysical controls on the stratocumulus topped boundary-layer structure during VOCALS-REx. *Atmos. Chem. Phys.*, **12**, 2849–2863, doi:10.5194/acp-12-2849-2012.

——, ——, P. Hill, and C. Morcrette, 2014a: Spatial variability of liquid cloud and rain: Observations and microphysical effects. *Quart. J. Roy. Meteor. Soc.*, **140**, 583–594, doi:10.1002/qj.2140.

——, J. Eyre, and A. Lock, 2014b: Seamless stratocumulus simulation across the turbulent gray zone. *Mon. Wea. Rev.*, **142**, 1655–1668, doi:10.1175/MWR-D-13-00229.1.

Bretherton, C. S., R. Wood, R. C. George, D. Leon, G. Allen, and X. Zheng, 2010: Southeast Pacific stratocumulus clouds, precipitation, and boundary layer structure sampled along 20°S during VOCALS-REx. *Atmos. Chem. Phys.*, **10**, 10 639–10 654, doi:10.5194/acp-10-10639-2010.

Burk, S. D., and W. T. Thompson, 1989: A vertically nested regional numerical weather prediction model with second-order closure physics. *Mon. Wea. Rev.*, **117**, 2305–2324, doi:10.1175/1520-0493(1989)117<2305:AVNRNW>2.0.CO;2.

Burleyson, C. D., S. P. deSzoeke, S. E. Yuter, M. Wilbanks, and W. A. Brewer, 2013: Ship-based observations of the diurnal cycle of southeast Pacific marine stratocumulus clouds and precipitation. *J. Atmos. Sci.*, **70**, 3876–3894, doi:10.1175/JAS-D-13-01.1.

Chen, C., and W. R. Cotton, 1987: The physics of the marine stratocumulus-capped mixed layer. *J. Atmos. Sci.*, **44**, 2951–2977, doi:10.1175/1520-0469(1987)044<2951:TPOTMS>2.0.CO;2.

Comstock, K. K., R. Wood, S. E. Yuter, and C. S. Bretherton, 2004: Reflectivity and rain rate in and below drizzling stratocumulus. *Quart. J. Roy. Meteor. Soc.*, **130**, 2891–2918, doi:10.1256/qj.03.187.

——, C. S. Bretherton, and S. E. Yuter, 2005: Mesoscale variability and drizzle in southeast Pacific stratocumulus. *J. Atmos. Sci.*, **62**, 3792–3807, doi:10.1175/JAS3567.1.

Davies, H. C., 1983: Limitations of some common lateral boundary schemes used in regional NWP models. *Mon. Wea. Rev.*, **111**, 1002–1012, doi:10.1175/1520-0493(1983)111<1002:LOSCLB>2.0.CO;2.

de Szoeke, S. P., S. E. Yuter, P. Zuidema, C. W. Fairall, and W. A. Brewer, 2010: Ship-based observation of drizzling stratocumulus clouds from EPIC to VOCALS. CLIVAR Exchanges, No. 39, International CLIVAR Project Office, Southampton, United Kingdom,11–13.

——, ——, D. Mechem, C. W. Fairall, C. D. Burleyson, and P. Zuidema, 2012: Observations of stratocumulus clouds and their effect on the eastern Pacific surface heat budget along 20°S. *J. Climate*, **25**, 8542–8567, doi:10.1175/JCLI-D-11-00618.1.

Fu, Q., and K. N. Liou, 1992: On the correlated k-distribution method for radiative transfer in nonhomogeneous

atmospheres. *J. Atmos. Sci.*, **49**, 2139–2156, doi:10.1175/1520-0469(1992)049<2139:OTCDMF>2.0.CO;2.

Garreaud, R. D., and R. Muñoz, 2004: The diurnal cycle in circulation and cloudiness over the subtropical South Pacific: A modeling study. *J. Climate*, **17**, 1699–1710, doi:10.1175/1520-0442(2004)017<1699:TDCICA>2.0.CO;2.

Geoffroy, O., J.-L. Brenguier, and I. Sandu, 2008: Relationship between drizzle rate, liquid water path, and droplet concentration at the scale of a stratocumulus cloud system. *Atmos. Chem. Phys.*, **8**, 4641–4654, doi:10.5194/acp-8-4641-2008.

Hill, A., B. Shipway, and I. Boutle, 2015: How sensitive are aerosol-precipitation interactions to the warm rain representation? *J. Adv. Model. Earth Syst.*, **7**, 987–1004, doi:10.1002/2014MS000422.

Hodur, R., 1997: The Naval Research Laboratory's Coupled Ocean/Atmosphere Mesoscale Prediction System (COAMPS). *Mon. Wea. Rev.*, **125**, 1414–1430, doi:10.1175/1520-0493(1997)125<1414:TNRLSC>2.0.CO;2.

Hogg, D. C., F. O. Guiraud, J. B. Snider, M. T. Decker, and E. R. Westwater, 1983: A steerable dual-channel microwave radiometer for measurement of water vapor and liquid in the troposphere. *J. Climate Appl. Meteor.*, **22**, 789–806, doi:10.1175/1520-0450(1983)022<0789:ASDCMR>2.0.CO;2.

Hudson, J. G., S. Noble, V. Jha, and S. Mishra, 2009: Correlations of small cumuli droplet and drizzle drop concentrations with cloud condenstaion nuclei concentrations. *J. Geophys. Res.*, **114**, D05201, doi:10.1029/2008JD010581.

——, ——, and ——, 2010: Stratus cloud supersaturations. *Geophys. Res. Lett.*, **37**, L21813, doi:10.1029/2010GL045197.

Justice, C. O., and Coauthors, 1998: The Moderate Resolution Imaging Spectroradiometer (MODIS): Land remote sensing for global change research. *IEEE Trans. Geosci. Remote Sens.*, **36**, 1228–1249, doi:10.1109/36.701075.

Kain, J. S., and J. M. Fritsch, 1990: A one-dimensional entraining/detraining plume model and its application in convective parameterization. *J. Atmos. Sci.*, **47**, 2784–2802, doi:10.1175/1520-0469(1990)047<2784:AODEPM>2.0.CO;2.

Kessler, E., 1969: *On the Distribution and Continuity of Water Substance in Atmospheric Circulations. Meteor. Monogr.*, No. 32. Amer. Meteor. Soc., 84 pp.

——, 1995: On the continuity and distribution of water substance in atmospheric circulations. *Atmos. Res.*, **38**, 109–145, doi:10.1016/0169-8095(94)00090-Z.

Khairoutdinov, M. F., and Y. L. Kogan, 2000: A new cloud physics parameterization for large-eddy simulation models of marine stratocumulus. *Mon. Wea. Rev.*, **128**, 229–243, doi:10.1175/1520-0493(2000)128<0229:ANCPPI>2.0.CO;2.

Klein, S. A., and D. L. Hartmann, 1993: The seasonal cycle of low stratiform clouds. *J. Climate*, **6**, 1587–1606, doi:10.1175/1520-0442(1993)006<1587:TSCOLS>2.0.CO;2.

Kogan, Y. L., 2013: A cumulus cloud microphysics parameterization for cloud-resolving models. *J. Atmos. Sci.*, **70**, 1423–1436, doi:10.1175/JAS-D-12-0183.1.

——, and D. B. Mechem, 2014: A PDF-based microphysics parameterization for shallow cumulus clouds. *J. Atmos. Sci.*, **71**, 1070–1089, doi:10.1175/JAS-D-13-0193.1.

Krueger, S. K., G. T. McLean, and Q. Fu, 1995: Numerical simulations of the stratus-to-cumulus transition in the subtropical marine boundary layer. Part I: Boundary-layer structure. *J. Atmos. Sci.*, **52**, 2839–2850, doi:10.1175/1520-0469(1995)052<2839:NSOTST>2.0.CO;2.

Larson, V. E., R. Wood, P. R. Field, J.-C. Golaz, T. H. Vonder Haar, and W. R. Cotton, 2001: Systematic biases in the microphysics and thermodynamics of numerical models that ignore subgrid-scale variability. *J. Atmos. Sci.*, **58**, 1117–1128, doi:10.1175/1520-0469(2001)058<1117:SBITMA>2.0.CO;2.

Leach, M. J., and S. Raman, 1995: Role of radiative transfer in maintenance and destruction of stratocumulus clouds. *Atmos. Environ.*, **29**, 2009–2018, doi:10.1016/1352-2310(94)00242-D.

Liu, M., J. E. Nachamkin, and D. L. Westphal, 2009: On the improvement of COAMPS weather forecasts using an advanced radiative transfer model. *Wea. Forecasting*, **24**, 286–306, doi:10.1175/2008WAF2222137.1.

Liu, Y., and P. H. Daum, 2004: Parameterization of the autoconversion process. Part I: Analytical formulation of the Kessler-type parameterizations. *J. Atmos. Sci.*, **61**, 1539–1548, doi:10.1175/1520-0469(2004)061<1539:POTAPI>2.0.CO;2.

——, ——, and R. L. McGraw, 2005: Parameterization of the autoconversion process: Kessler-type, Sundqvist-type, and unification. *Proc. 15th ARM Science Team Meeting*, Daytona Beach, FL, ARM Program, 8 pp. [Available online at https://www.arm.gov/publications/proceedings/conf15/extended_abs/liu_y.pdf.]

Louis, J., M. Tiedtke, and J. F. Geleyn, 1982: A short history of the operational PBL—Parameterization at ECMWF. *Proc. Workshop on Planetary Boundary Layer Parameterization*, Reading, United Kingdom, ECMWF, 59–79. [Available online at http://www.ecmwf.int/sites/default/files/elibrary/1982/10845-short-history-pbl-parameterization-ecmwf.pdf.]

Manton, M. J., and W. R. Cotton, 1977: Parameterization of the atmospheric surface layer. *J. Atmos. Sci.*, **34**, 331–334, doi:10.1175/1520-0469(1977)034<0331:POTASL>2.0.CO;2.

McCaa, J. R., and C. S. Bretherton, 2004: A new parameterization for shallow cumulus convection and its application to marine subtropical cloud-topped boundary layers. Part II: Regional simulations of marine boundary layer clouds. *Mon. Wea. Rev.*, **132**, 883–896, doi:10.1175/1520-0493(2004)132<0883:ANPFSC>2.0.CO;2.

Mechem, D. B., and Y. L. Kogan, 2003: Simulatin the transition from drizzling marine stratocumulus to boundary layer cumulus with a mesoscale model. *Mon. Wea. Rev.*, **131**, 2342–2360, doi:10.1175/1520-0493(2003)131<2342:STTFDM>2.0.CO;2.

——, and ——, 2008: A bulk parameterization of giant CCN. *J. Atmos. Sci.*, **65**, 2458–2466, doi:10.1175/2007JAS2502.1.

——, P. C. Robinson, and Y. L. Kogan, 2006: Processing of cloud condensation nuclei by collision-coalescence in a mesoscale model. *J. Geophys. Res.*, **111**, D18204, doi:10.1029/2006JD007183.

Mechoso, C. R., and Coauthors, 2014: Ocean–cloud–atmosphere–land interactions in the southeastern Pacific: The VOCALS program. *Bull. Amer. Meteor. Soc.*, **95**, 357–375, doi:10.1175/BAMS-D-11-00246.1.

Medeiros, B., B. Stevens, I. M. Held, M. Zhao, D. L. Williamson, J. G. Olson, and C. S. Bretherton, 2008: Aquaplanets, climate sensitivity, and low clouds. *J. Climate*, **21**, 4974–4991, doi:10.1175/2008JCLI1995.1.

Mellor, G. L., and T. Yamada, 1982: Development of a turbulence closure model for geophysical fluid problems. *Rev. Geophys.*, **20**, 851–875, doi:10.1029/RG020i004p00851.

Morrison, H., J. A. Curry, and V. I. Khvorostyanov, 2005a: A new double-moment microphysics parameterization for application in cloud and climate models. Part I: Description. *J. Atmos. Sci.*, **62**, 1665–1677, doi:10.1175/JAS3446.1.

——, ——, M. D. Shupe, and P. Zuidema, 2005b: A new double-moment microphysics parameterization for application in cloud and climate models. Part II: Single-column modeling of

arctic clouds. *J. Atmos. Sci.*, **62**, 1678–1693, doi:10.1175/JAS3447.1.

Painemal, D., and P. Zuidema, 2011: Assessment of MODIS cloud effective radius and optical thickness retrievals over the southeast Pacific with VOCALS-REx in situ measurements. *J. Geophys. Res.*, **116**, D24206, doi:10.1029/2011JD016155.

Pincus, R., and S. A. Klein, 2000: Unresolved spatial variability and microphysical process rates in large-scale models. *J. Geophys. Res.*, **105**, 27 059–27 065, doi:10.1029/2000JD900504.

Platnick, S., M. D. King, S. A. Ackerman, W. P. Menzel, B. A. Baum, J. C. Ridi, and R. A. Frey, 2003: The MODIS cloud products: Algorithms and examples from Terra. *IEEE Trans. Geosci. Remote Sens.*, **41**, 459–473, doi:10.1109/TGRS.2002.808301.

Rahn, D. A., and R. Garreaud, 2010a: Marine boundary layer over the subtropical southeast Pacific during VOCALS-REx. Part 1: Mean structure and diurnal cycle. *Atmos. Chem. Phys.*, **10**, 4491–4506, doi:10.5194/acp-10-4491-2010.

——, and ——, 2010b: Marine boundary layer over the subtropical southeast Pacific during VOCALS-Rex. Part 2: Synoptic variability. *Atmos. Chem. Phys.*, **10**, 4507–4519, doi:10.5194/acp-10-4507-2010.

Remer, L. A., and Coauthors, 2005: The MODIS aerosol algorithm, products, and validation. *J. Atmos. Sci.*, **62**, 947–973, doi:10.1175/JAS3385.1.

Rogers, R. R., and M. Yau, 1989: A *Short Course* in *Cloud Physics*. 3rd ed. International Series in Natural Philosophy, Vol. 113, Butterworth Heinemann, 304 pp.

Rutledge, S. A., and P. V. Hobbs, 1983: The mesoscale and microscale structure and organization of clouds and precipitation in midlatitude cyclones. VIII: A model for the "seeder-feeder" process in warm-frontal rainbands. *J. Atmos. Sci.*, **40**, 1185–1206, doi:10.1175/1520-0469(1983)040<1185:TMAMSA>2.0.CO;2.

Seifert, A., and K. D. Beheng, 2006: A two-moment cloud microphysics parameterization for mixed-phase clouds. Part 2: Maritime vs. continental deep convective storms. *Meteor. Atmos. Phys.*, **92**, 67–82, doi:10.1007/s00703-005-0113-3.

Stevens, B., 2005: Atmospheric moist convection. *Annu. Rev. Earth Planet. Sci.*, **33**, 605–643, doi:10.1146/annurev.earth.33.092203.122658.

——, W. R. Cotton, G. Feingold, and C.-H. Moeng, 1998: Large-eddy simulations of strongly precipitating, shallow, stratocumulus-topped boundary layers. *J. Atmos. Sci.*, **55**, 3616–3638, doi:10.1175/1520-0469(1998)055<3616:LESOSP>2.0.CO;2.

IPCC, 2013: *Climate Change 2013: The Physical Science Basis*. Cambridge University Press, 1535 pp., doi:10.1017/CBO9781107415324.

Toniazzo, T., S. J. Abel, R. Wood, C. R. Mechoso, G. Allen, and L. C. Shaffrey, 2011: Large-scale and synoptic meteorology in the south-east Pacific during the observations campaign VOCALS-REx in austral spring 2008. *Atmos. Chem. Phys.*, **11**, 4977–5009, doi:10.5194/acp-11-4977-2011.

van Zanten, M. C., B. Stevens, G. Vali, and D. H. Lenschow, 2005: Observations of drizzle in nocturnal marine stratocumulus. *J. Atmos. Sci.*, **62**, 88–106, doi:10.1175/JAS-3355.1.

Wang, S., L. W. O'Neil, Q. Jiang, S. P. de Szoeke, X. Hong, H. Jin, W. T. Thompson, and X. Zheng, 2011: A regional real-time forecast of marine boundary layers during VOCALS-REx. *Atmos. Chem. Phys.*, **11**, 421–437, doi:10.5194/acp-11-421-2011.

Wood, R., 2005: Drizzle in stratiform boundary layer clouds. Part II: Microphysical aspects. *J. Atmos. Sci.*, **62**, 3034–3050, doi:10.1175/JAS3530.1.

——, 2006: Rate of loss of cloud droplets by coalescence in warm clouds. *J. Geophys. Res.*, **111**, D21205, doi:10.1029/2006JD007553.

——, P. Field, and W. Cotton, 2002: Autoconversion rate bias in stratiform boundary layer cloud parameterizations. *Atmos. Res.*, **65**, 109–128, doi:10.1016/S0169-8095(02)00071-6.

——, M. Köhler, R. Bennartz, and C. O'Dell, 2009: The diurnal cycle of surface divergence over the global oceans. *Quart. J. Roy. Meteor. Soc.*, **135**, 1484–1493, doi:10.1002/qj.451.

——, and Coauthors, 2011: The VAMOS Ocean–Cloud–Atmosphere–Land Study Regional Experiment (VOCALS–REx): Goals, platforms, and field operations. *Atmos. Chem. Phys.*, **11**, 627–654, doi:10.5194/acp-11-627-2011.

Wyant, M. C., and Coauthors, 2010: The PreVOCA experiment: Modeling the lower troposphere in the Southeast Pacific. *Atmos. Chem. Phys.*, **10**, 4757–4774, doi:10.5194/acp-10-4757-2010.

——, and Coauthors, 2015: Global and regional modeling of clouds and aerosols in the marine boundary layer during VOCALS: The VOCA intercomparison. *Atmos. Chem. Phys.*, **15**, 153–172, doi:10.5194/acp-15-153-2015.

Zuidema, P., E. R. Westwater, C. Fairall, and D. Hazen, 2005: Ship-based liquid water path estimates in marine stratocumulus. *J. Geophys. Res.*, **110**, D20206, doi:10.1029/2005JD005833.